Hindawi
Mathematical Problems in Engineering
Volume 2024, Article ID 8922303, 16 pages
https://doi.org/10.1155/2024/8922303

Research Article

Post-Fracture Stiffness and Residual Capacity Assessment of Film-Retrofitted Monolithic Glass Elements by Frequency Change

Chiara Bedon and Marco Fasan

Department of Engineering and Architecture, University of Trieste, Trieste, Italy

Correspondence should be addressed to Chiara Bedon; chiara.bedon@dia.units.it

Received 12 October 2023; Revised 20 January 2024; Accepted 22 February 2024; Published 1 March 2024

Academic Editor: Francesco Foti

The primary goal of safety films for glass in buildings is to retrofit existing monolithic elements and prevent, in the post-fracture stage, any fall-out of shards. Their added value is that—as far as the fragments are kept bonded—a cracked film-glass element can ensure a minimum residual mechanical and load-bearing capacity, which is strictly related to the shards interlocking and debond. To prevent critical issues, such a mechanical characterization is both important and uncertain, and requires specific methodologies. In this regard, a dynamic investigation is carried out on fractured film-bonded glass samples, to assess their post-fracture stiffness trends and its sensitivity to repeated vibrations. The adopted laboratory layout is chosen to assess the effects of random vibrations (220 repetitions) on a total of 12 cracked specimens in a cantilever setup (with 0.5–5 m/s^2 the range of randomly imposed acceleration peaks). By monitoring the cracked vibration frequency, the film efficiency and corresponding residual bending stiffness of cracked glass samples are quantified as a function of damage severity, with a focus on fragments interlock. Quantitative experimental estimates are comparatively analyzed and validated with the support of finite element (FE) numerical models and analytical calculations. As shown—at least at the small-scale level—a progressive post-fracture stiffness reduction takes place under repeated random vibrations, and this implicitly affects the residual load-bearing capacity of glass members. Most importantly, for the tested configurations, it is shown that the cracked vibration frequency is minimally affected by crack geometry, and follows a rather linear decrease with the number of imposed random impacts (up to an average of ≈20 for each sample), thus confirming the retrofit potential and efficiency in providing some mechanical capacity through fragments interlock.

1. Introduction

Structural glass applications in buildings are based on design concepts that are voted to avoid possible fracture and based on robustness and redundancy concepts—minimize possible risks for people, in case of partial/severe damage [1, 2]. In this context, a key role is usually assigned to several types and solutions of the connections, that can be optimally designed by taking advantage of mechanical joints [3], adhesive bonds and viscoelastic materials [4], or even hybrid technologies [3]. To improve the structural efficiency and minimize possible damage, literature studies in the field of structural glass and glass-related bonded components include deep investigations on durability aspects [5], mechanical effects of aging phenomena [6], or repeated thermal gradients [7], and methods to assess the residual capacity of bonds in existing glass systems [8]. Special efforts are spent also for the load-bearing capacity assessment of embedded metal connections [9], with many investigations aimed at supporting the quantification/optimization of their residual mechanical efficiency under long-term effects [10], temperature variations [11], and post-critical interlock with fractured glass [12]. Due to the basic brittleness of glass [1, 2, 13]—as also highlighted by literature experimental and numerical studies like [9–12]—bonded components and connections require a major attention both for the elastic characterization and for the analysis/prevention of failure mechanisms, in order to ensure sufficient residual capacity and robustness in case of damage.

The residual capacity preservation in case of unfavorable conditions or even accidental actions and events (like impacts [14, 15]) is a relevant issue for newly designed glass systems but especially for existing ones, which have been constructed

Figure 1: Examples of fractured glass windows. Reproduced from PxHere (CC0 license).

without the technical support of recent design standards and specifications (i.e., [1, 2]), and are consequently characterized —in most of cases—by load-bearing and post-fracture criticalities [15]. In case of special performance needs, among others, the use of covering films for glass represents an open research and industrial challenge characterized by the multifunctional potentials, including thermal [16] and corrosion [17] benefits. In terms of structural safety, anti-shatter films can support the post-fracture stage, as they can prevent the spread of critical shards from cracked monolithic glass components (Figure 1 and study by Figuli et al. [15]). Given that these films are typically used for post-fracture hazard minimization, but are characterized by the small thickness, very limited bending stiffness, and uncertain adhesion properties, an open question is represented by the quantification of their mechanical potential in keeping glass fragments together, especially under aging or unfavorable conditions [18–20]. Among others, debonding and fall-out of glass shards [21, 22] would in fact result in major consequences for glass section, and thus for the customers.

In this study, the attention is focused on the post-fracture characterization of bonded fragments, and on the effects of imposed repeated vibrations on film-retrofitted monolithic glass samples, so as to quantify their expected residual stiffness after first breakage. The reason is that—as it happens for many structural engineering applications [23–25]—repeated vibrations are known to strongly affect the retrofit durability and efficiency. When the retrofit intervention takes the form of bonded safety films applied to typically brittle in tension elements like glass, any possible sensitivity to mechanical loads can have major consequences on the associated safety levels. In parallel, it is of utmost importance to define practical strategies and tools to quantify these residual load-bearing performances and safety levels.

In this regard, an original experimental investigation is carried out in this paper, to capture the mechanical features/capacity of fractured film-retrofitted glass samples. The cracked vibration frequency of samples is tracked as a key performance indicator. Frequency changes in simple beams or cantilevers are in fact well-known to represent a meaningful parameter for the structural analysis of crack members, and a large number of theoretical, experimental, or numerical studies can be found in the literature. Most of them are aimed at providing robust support for diagnostic purposes, like elaborating a sound mathematical description of the cracked behavior of members [26], or developing simplified analytical models [27, 28], or even assessing different theoretical models for multiple crack configurations in simple members [29–32].

Certainly, model updating can also provide a robust support to the experimental interpretation of damage/crack severity in load-bearing elements [33]. Several literature studies proved that both direct and indirect (inverse) methods can offer high accuracy for the analysis of cracked members [34], and efficiently support the detection/quantification of crack shape and size effects [29, 35]. According to Bedon [22], Zhang et al. [36–38], and others, it is worth to note that the fundamental vibration frequency and its possible variation can be used not only for a prompt crack detection, but also for to quantify possible delamination phenomena, which are particularly critical for those composite elements and systems (like film-retrofitted glass elements) affected by partial/progressive debonding. Several modeling approaches [39], in this regard, confirm that the damage severity can be quantitatively correlated to the stiffness losses.

Following the above considerations, the present investigation focuses on the dynamic characterization of small-scale samples consisting of a fractured monolithic glass plate with fragments bonded by antishatter film. To verify the proposed experimental strategy, a commercial safety film based on polyethylene terephthalate (PET)-layers and pressure sensitive adhesives (PSAs) is taken into account, with mechanical and thermo-physical properties as in [18–20]. By taking an advantage of previous experimental efforts at the material characterization level [18–20], the primary goal of current investigation is represented by the experimental characterization of cracked glass-film composite samples in cantilever setup and subjected to the random repeated vibrations. Based on vibration frequency analysis, their residual post-fracture stiffness and mechanical capacity is tracked and measured. The cantilever-like setup is chosen because representative—under small-scale simplifications—of fracture features that are typical of real monolithic glass elements in buildings. As in the examples of Figure 1, cracked glass elements can in fact possibly take advantage of some interlock of the major fragments, and thus offer a minimum load-bearing capacity, as far as these fragments are kept in position and bonded by the safety films.

2. Methodology and Background

Measuring the capacity of existing film-bonded glass elements is rather challenging, but of utmost importance for

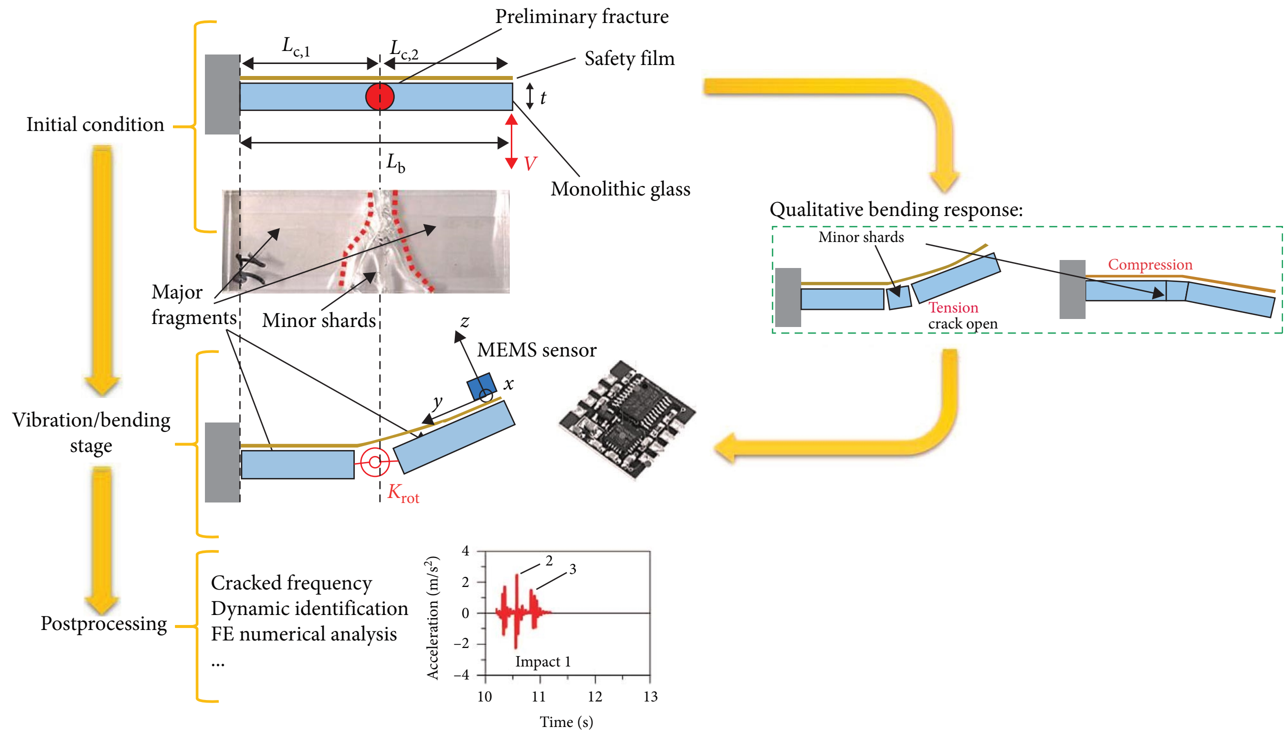

Figure 2: Schematic setup and operational steps for the current experimental investigation (with $L = 100$ mm, $L_b = 95$ mm, $t = 6$ mm, and $L_{c,1} \approx 0.5\ L_b$).

safety prevention. The present investigation, in this sense, takes a major advantage from laboratory experiments carried out on fractured film-retrofitted monolithic glass samples. In parallel, further insight is also derived from a robust finite element (FE) analysis, developed to extend the experimental findings and analyze the film-to–glass interaction (i.e., shards interlock), with a focus on its effects on the corresponding cracked vibration frequency $f_{1,\mathrm{cr}}$.

Overall, the experimental analysis is based on a test setup like in Figure 2, which schematically reproduces the typical cantilever layout and an example of measured accelerations records in time (for the mechanical characterization of the system in free vibrations). To note that each sample was prepared as in Section 3.

In Figure 2, the safety film is used to bond the preliminary fractured glass sample (with $L_{c,1} \approx 0.5\ L_b$ the distance of the crack from the fixed end). Under the imposed repeated vibrations, the dynamic response of each sample is tracked by means of a triaxial MEMS sensor (accelerometer + inclinometer), which is used (at the free cantilever end) to characterize the post-fracture effective bending stiffness. To facilitate the analysis of results, the fixed end of glass is rigidly clamped to the test setup.

The schematic drawing of Figure 2, more in detail, emphasizes both the instrument layout and the expected bending behavior of film-retrofitted glass samples in free vibrations. For their dynamic analysis and characterization, it is assumed that the two major glass fragments can mechanically interact until the minor interposed shards offer a minimum structural continuity to the cantilever, thanks to the bonding film. Such a specific damage scenario was reproduced—in laboratory conditions—to investigate the typical shard interlock (by contact mechanisms), and its sensitivity to repeated impacts/vibrations. A major uncertainty for the dynamic characterization of fractured glass elements—compared to the other constructional members—is in fact strictly related to interlocking. For the same reason, the safety film was bonded on the top side of cracked cantilevers, so as to facilitate (on the conservative side) any possible fall-out of glass shards during the test repetitions. Under repeated vibrations [18], it is worth to remind that the tensile side mechanism of Figure 2 (i.e., crack opening) represents the most influencing stage for the dynamic assessment of tested samples, and it has consequently major effects on the measured $f_{1,\mathrm{cr}}$ value.

The open challenge for the experimental samples as in Figure 2 is thus represented by the prediction of the actual post-fracture bending stiffness and its possible loss under random vibrations. Also, major laboratory outcomes can be exploited by the dynamic identification of fractured samples [38, 39]. To track the most important dynamic parameters in the cracked stage, according to literature [26–30], a simple and efficient modeling strategy could be developed by introducing an equivalent spring with stiffness K_{rot} (Figure 2), which is assumed to reproduce the effects of shards interlock in the region of major crack. For the application of a similar model to fractured glass, more in detail, K_{rot} should reproduce the physical contact of fragments in bending with the limit values of null stiffness in tension ($K_{\mathrm{rot}} = 0$ when minor fragments are open) and rigid stiffness in compression ($K_{\mathrm{rot}} = \infty$ for the compressed glass fragments in contact). Among various performance indicators, the interpretation of experimental results is basically exploited in terms of $f_{1,\mathrm{cr}}$, and further elaborated by the parametric FE simulations [40].

The basic assumption is in fact that a clamped glass sample with monolithic t thick section, lumped mass sensor (M_s) at its free end, and a test setup like in Figure 2, the fundamental uncracked vibration frequency f_1 is [41, 42] as follows:

$$f_1 = \frac{1}{2\pi}\sqrt{\frac{3EJ}{M_{\mathrm{eff}}L_b^3}}, \tag{1}$$

with M_{eff} the effective mass given by:

$$M_{\mathrm{eff}} = \frac{33}{140}\left(M_g + M_f\right) + M_s, \tag{2}$$

where M_g and M_f denote the mass of glass plate and film tape, while L_b is the actual bending span.

Assuming that the bonding film has minimum bending stiffness (with 0.35 mm its thickness [18–20], $M_f = 0.3969$ g ≈ 0 and $E_f = 8.1$ MPa), f_1 in Equation (1) mostly depends on the Young's modulus $E = 70$ GPa of glass, on the second moment of area J of the uncracked $B \times t$ glass section, and on the corresponding bending stiffness EJ. To note that the analytical results from Equation (1) represent an ideal upper limit for the tested cantilever samples, which in real constructions may be generally affected by the possible support flexibility (if any) or degradation (if any), delamination (in case of laminated sections), glass fracture (as in the present analysis), etc., with major effects on the final dynamic performances [22, 38].

In case of a major crack with depth a and distance $L_{c,1}$ from the fixed end, see Figure 2, the cracked fundamental frequency is as follows:

$$f_{1,\mathrm{cr}} < f_1, \tag{3}$$

and is sensitive to several well-known crack features, such as its position, depth, size, etc.

For cracked monolithic glass elements, a primary role is thus given to the bonding film.

Assuming that the crack has propagation $a = 0 - t$ through the thickness t of a given specimen as in Figure 2, Equation (3) could take various established analytical forms [26–30]. For the present investigation, the basic assumption is that $a/t = 1$ at the initial stage of vibration tests, and minor glass fragments are kept bonded in position by the safety film.

3. Experimental Investigation

3.1. Characteristics and Preparation of Specimens. The typical small-scale specimen consisted of a monolithic, annealed glass plate with $L = 100 \times B = 40 \times t = 6$ mm dimensions. The use of monolithic and float glass was privileged to facilitate the computational process (i.e., lack of possible viscoelastic phenomena of interlayers, debonding, etc.). The limited thickness t and typical fracture behavior of annealed glass, moreover, was chosen to ensure the presence of cracks with $a/t = 1$ for all the tested samples. The difference among specimens was represented by minor/scattered variations in the size and shape of fragments in the region of fracture (with $a/t = 1$), which are also typical of glass cracking mechanisms. A commercial multilayer film characterized by 0.35 mm total thickness was used to keep in position these fragments (Figure 2). The selected film is composed by two different layers made of PET, with a thickness of 0.11 and 0.22 mm, respectively, and a PSA adhesive that was preliminary protected by the environmental conditions by means of a removable release liner [18–20]. At the assembly stage, the glass specimens were bonded to 35 mm in width and 120 mm in length strips.

To facilitate the manual operations, the film was cut in 120 mm long tapes, and then positioned to span 20 mm from the free end. The preparation was based on the dry lamination procedure. The strip was applied on the rigid glass sample with high pressure, in order to make it perfectly adherent. The adhesion stage was realized with careful attention to avoid bubbles and superficial folding. To minimize the influence of little impurities or inclusions, the glass surface was treated and the protection film was quickly peeled off. Then, manual pressure was applied to the film to remove any residual heterogeneity and to make the adhesion as homogeneous as possible.

Before the execution of dynamic experiments, a preliminary crack like in Figure 2 was imposed to the glass-film samples, by hammer hit. The steel hammer was used to fracture all the glass elements around their midspan region, so as to create a major crack (with $a/t = 1$ and $L_{c,1} = 0.5\ L_b$) and minor scattered shards around midspan.

Figure 3 shows typical examples of film-retrofitted glass samples, as arranged for the present experimental analysis. Compared to the preliminary stage with the uncracked assembly (Figure 3(a)), a major crack artificially created as in Figure 3(b) was used as reference configuration for the initial testing stage. Each sample consisted consequently of (i) two major glass fragments, (ii) few minor glass shards in the region of crack, and (iii) the bonding safety film. Each sample was subjected to several test repetitions, where each one consisted in a random finger tap (Section 3.2). To note, as reported in Figure 3(b), that the test repetitions were typically associated to partial fall-out of millimetric glass fragments from the region of crack, due to the progressive interlock of the bonded shards. While this phenomenon was rationally characterized by negligible mass reduction of glass, a minimum debonding of shards was expected due to the multiple imposed vibrations. Under progressive damage propagation, as a major consequence of negligible out-of-plane stiffness of the safety film alone, the performed test repetitions were aborted at the first occurrence of severe debonding of minor shards from the cracked region (see for example Figures 3(d) and 3(e)), i.e., due to lack of residual bending rigidity, mechanical continuity, and cantilever behavior for

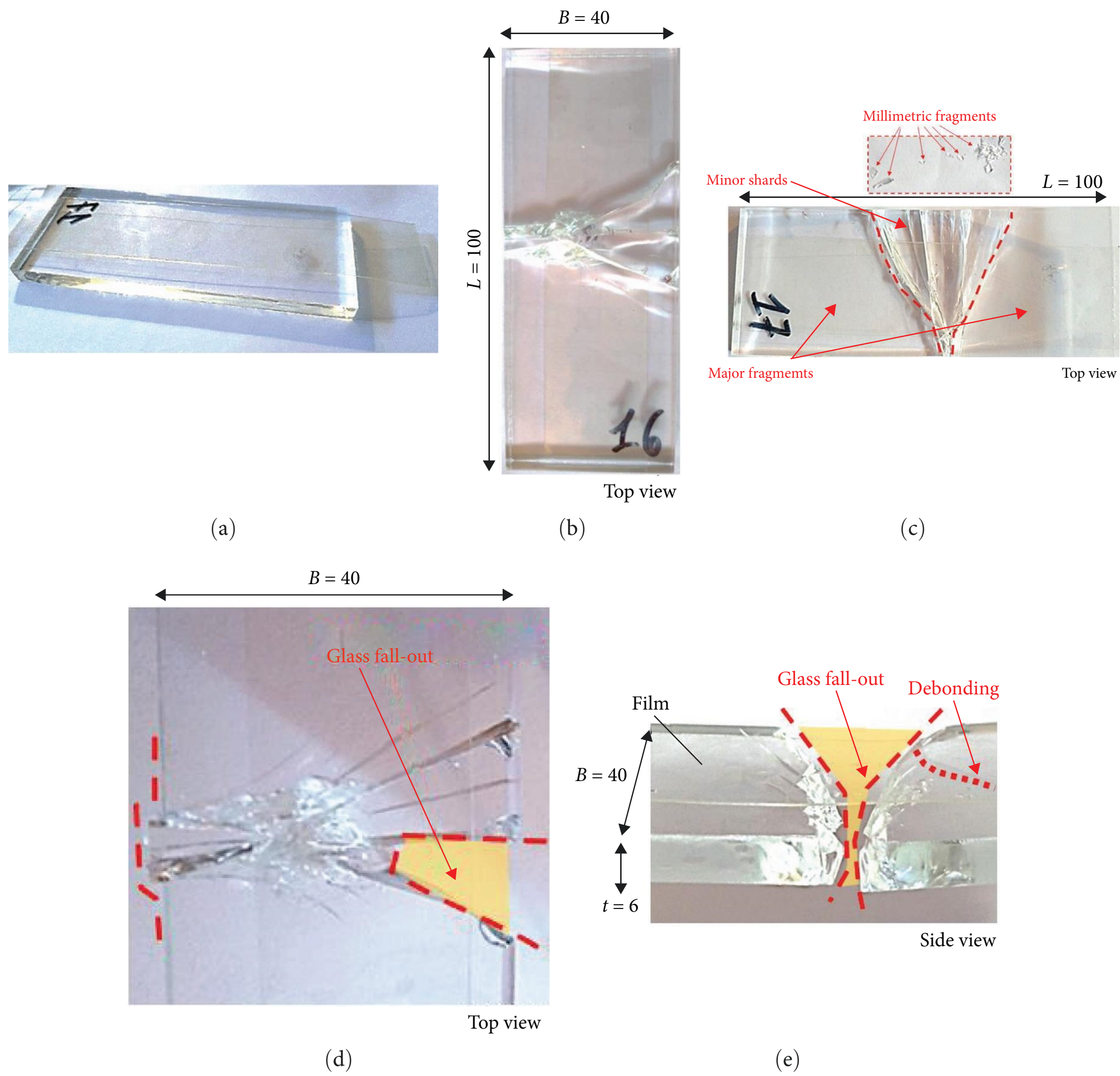

Figure 3: Example of presently investigated film-retrofitted glass specimens: (a) initial configuration (axonometry) and (b) deliberately cracked scenario (before/at the beginning of dynamic tests); (c) fall-out of millimetric glass fragments (during tests); (d, e) final configuration (after tests) and evidence of major damage severity, due to several test repetitions and progressive debond of glass fragments. Dimensions in mm (out-of-scale photos, by ©C. Bedon).

the examined samples. In this sense, the key role of retrofit in preserving a minimum/temporary, partial contact mechanism for the interlocking glass shards was addressed.

3.2. Test Configurations. The average laboratory temperature at the time of experiments was measured in 30°C (Summer). The specimens were positioned in a clamped boundary configuration according to Figures 2 ("CC" setup, in the following). The depth of clamp restraint was set in 5 mm (thus resulting in $L_b = 95$ mm of bending span). Hardwood timber logs and steel plates were used on the top and bottom surfaces of glass, and rigidly fixed to reproduce an ideal clamp.

Each sample was subjected to small-amplitude, finger tap impacts to involve vibrations at the free end. These testing conditions were overall quantified in acceleration peaks in the range of 0.5–5 m/s^2.

A summary of test configurations is listed in Section 4, in the discussion of results. A set of 220 repetitions were elaborated for a number of 12 film-bonded specimens, all of them experimentally investigated under similar setup (Figure 2). According to Figures 3(b) and 3(c), each sample was preliminary cracked around the midspan region, by hammer. This choice resulted in variations in the shape/size of minor fragments (i.e., Figure 3(b)), but in a more realistic fracture scenario.

3.3. Instruments. The experimental study was based on classical dynamic identification techniques, which have been for example applied to glass specimens in [22, 38], and on the experimental characterization of safety films reported in [18–20]. For the setup in Figure 2, three-component acceleration histories were measured by MEMS sensor, with a

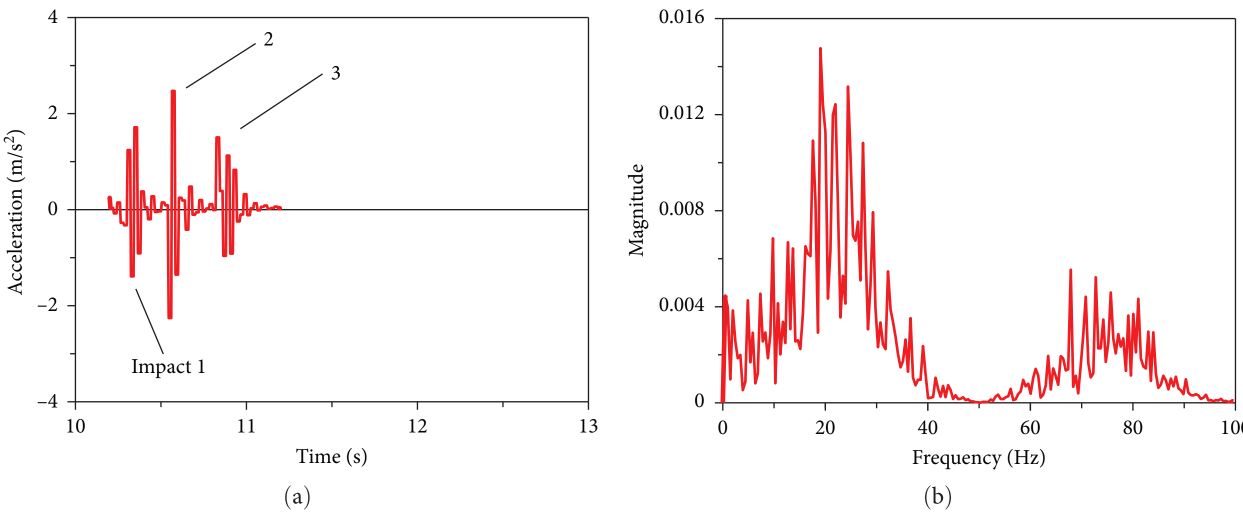

FIGURE 4: Example of current experimental measurements at the free end of fractured film-bonded cantilever glass samples under repeated vibrations (test setup as in Figure 2): (a) accelerations in time and (b) FFT spectra.

sampling rate of 200 Hz. Meanwhile, the rotation angle (in degrees) about a local reference system as in Figure 2 was also measured. The mini device consisted in a commercial sensor based on IMU AHRS MPU6050 chip board, wireless, three-axes accelerometer sensor with inclinometer (±16 g its range, 0.005 g the resolution, 0.2–200 Hz the available sampling rate). This commercial sensor is equipped by integrated battery and embedded microcontroller, ARM® Cortex®-M0 single core type (32 bit, clock frequency up to 48 MHz). The limited size of MEMS sensor (36mm × 36 mm, with 15 mm the thickness) was chosen to have minimum effects on the experimental setup and results. Also, its weight $M_s = 20$ g—although small—was taken into account as lumped mass at the free end of cantilever samples.

A typical experimental record is shown in Figure 4, in terms of acceleration component at the free end of cantilever under three consecutive impacts (with random imposed peaks, Figure 4(a)) and an example of fast Fourier transform (FFT) spectra (for single impact, Figure 4(b)).

For postprocessing, major elaborations and signal processing analyses on the available experimental records were carried out with the support of a Matlab® toolbox [43], in order to assess the cracked response of film-bonded monolithic glass samples as a function of input acceleration.

Based on the available MEMS sensor and the measured accelerations for all test repetitions, the dynamic response of each sample was studied with the support of the Structural Modal Identification Toolsuite software (SMIT). The ERA-OKID-OO approach was used for this purpose [44, 45], given that it is particularly efficient and stable for natural frequencies, damping ratios, vibration shapes estimation of all those vibrating systems whose initial conditions and dynamic external excitation are unknown. For the present investigation, the attention was primarily focused on the analysis of the cracked vibration frequency.

3.4. Numerical Investigation. To support the interpretation of experimental findings, a consolidated and efficient modeling strategy was taken into account for linear modal frequency analyses. A simplified FE model (Section 3.4.1) was in fact developed in ABAQUS/Standard [40], to reproduce the typical glass-film sample and estimate its cracked vibration frequency, by changing the equivalent spring stiffness K_{rot} as in Figure 2.

As a further validation, a geometrically accurate FE model was also assembled (Section 3.4.2), in order to reproduce more realistically the effect of minor shards and their interlock (based on the measured size of fragments in the experimental samples). This second model was used to verify the cracked bending response of samples, as well as the accuracy of the simplest model, and its possible limits for the predicted frequency trends.

3.4.1. Simplified Model. The major assumption to describe to the experimental samples like in Figure 3 consisted in a rough simplification of the nominal geometry of glass fragments.

Basically, the simplified FE model in Figure 5 included (i) two parts representative of major glass fragments, (ii) a set of interposed equivalent springs (K_{rot}), (iii) and a thin layer representative of the bonding film. The size/length of major fragments was defined based on the average measurement of samples, with $L_{c,1} = 0.5\ L_b$. Accordingly, the midspan gap was set in 10 mm, based on average experimental measurements (Figure 5(b)). Shell (S4R type) and brick elements (C3D8R type) were used for the glass and film components, respectively. A regular mesh pattern was defined for them, with a reference seed in the range of 0.35 mm and up to 1 mm. This choice resulted in 6,500 elements and 38,500° of freedom.

A rigid "tie" bond was used at the contact interface of glass and film parts (Figure 5(a)). This kinematic assumption was chosen to avoid relative translations and rotations of the interested nodes, and thus to support the prediction of a reference, ideal cracked vibration frequency $f_{1,\mathrm{cr}}$ for the tested samples. As in Figure 5(b), the bond surface was defined to span over the full length of major glass parts (L_{bond}).

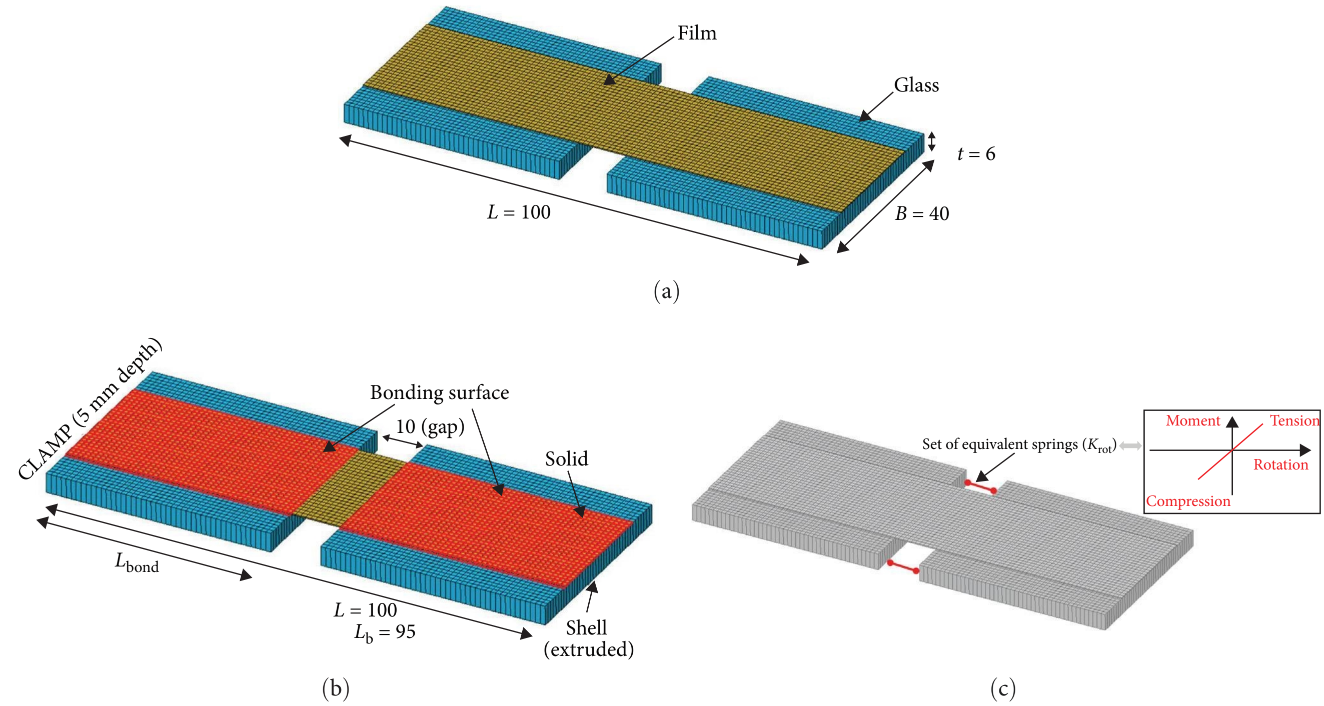

Figure 5: View of the simplified numerical model for cracked vibration frequency analysis (axonometric view, ABAQUS): (a) assembly; (b) geometry and bonding surfaces; and (c) equivalent springs for the cracked region. Dimensions in mm.

In between (midspan major crack), a set of rotational springs was used to account for interlock (Figure 5(c)). The input stiffness K_{rot} of these linear elastic springs was parametrically modified to assess the sensitivity of $f_{1,\text{cr}}$. Through the parametric study, the clamped end of glass was mechanically fixed by means of equivalent nodal restraints.

Input material properties for glass and film parts were described based on the linear elastic constitutive models. In case of annealed glass, the modulus of elasticity was set at $E = 70$ GPa, with $\nu = 0.23$ the Poisson' ratio and $\rho = 2{,}500$ kg/m^3 the material density [16]. The safety film was mechanically described based on the experimental characterization reported in [18], that is with $G_f = 3$ GPa the shear modulus, $\nu_f = 0.35$ the Poisson' ratio, and $\rho_f = 1{,}350$ kg/m^3 the density. The clamp restraint for the glass part was ideally reproduced at the fixed shell section, by means of distributed equivalent nodal restraints.

To note that the geometry and size of MEMS sensor at the free end of glass plate were neglected, but a lumped mass ($M_s = 20$ g) was placed at the midspan node. On the other side, the mass effect of millimetric glass fragments as in Figure 3(c) was disregarded. The mass contribution of minor glass shards associated to the artificial/numerical crack (gap) in the midspan section of glass plate ($\approx$6 g for the 10 mm thick gap, corresponding to $\approx 0.1\ M_g$ and $\Delta M = -10\%$) was included in simulations in the form of distributed lumped mass terms. Also in this case, it is relevant to observe that the simplified numerical assumption as in Figure 5 was described as a limit configuration of average experimental observations. The total mass of intact glass samples ($M_g = 59.76$ g), with the imposed midspan crack, was in fact typically affected by minor/negligible mass variations ΔM due to repeated vibrations and partial debonding of the small fragments (Figure 3(c)). After the conclusion of test repetitions, the average mass of minor glass shards associated to final fall-out was measured in about $\Delta M = -5\%$, and down to $\Delta M = -10\%$ for one specimen only (Figures 3(d) and 3(e)), which was considered for the modeling purposes.

3.4.2. Geometrically Accurate Model. As a further elaboration and validation from Section 3.4.1, solid brick elements (C3D83 type) were used for both the film part and the glass elements, including minor shards to replace the equivalent springs. In this way, possible interlock effects were further addressed. All the other model features, such as the "tie" surface-based kinematic constraint to bond film and glass, as well as the ideal clamp restraint, or the elastic material properties and the lumped mass contribution M_s of sensor, were again described as in Section 3.4.1.

Figure 6 shows a model detail and the typical fundamental modal shape. It can be seen in Figure 6(b) that the clamped glass fragment, as also expected from the experimental observations, is characterized by almost null deformations, while the out-of-plane bending shape of the film-bonded cantilever is characterized by a major slope variation and vertical deformation at the free end, as a consequence of shards interlock. Also, it can be noted from the legend values in Figure 6(b) that the vertical displacement (U3) of the model mostly coincides with its global deformation (U magnitude). As far as the minor shards are kept bonded by the safety film, a minimum residual bending stiffness for the cracked cantilever can be thus ensured.

4. Results

4.1. Analytical and Numerical Frequency Sensitivity to Major Crack. The attention was first focused on the quantification of $f_{1,\text{cr}}$ for the samples described in Figure 5, as a function

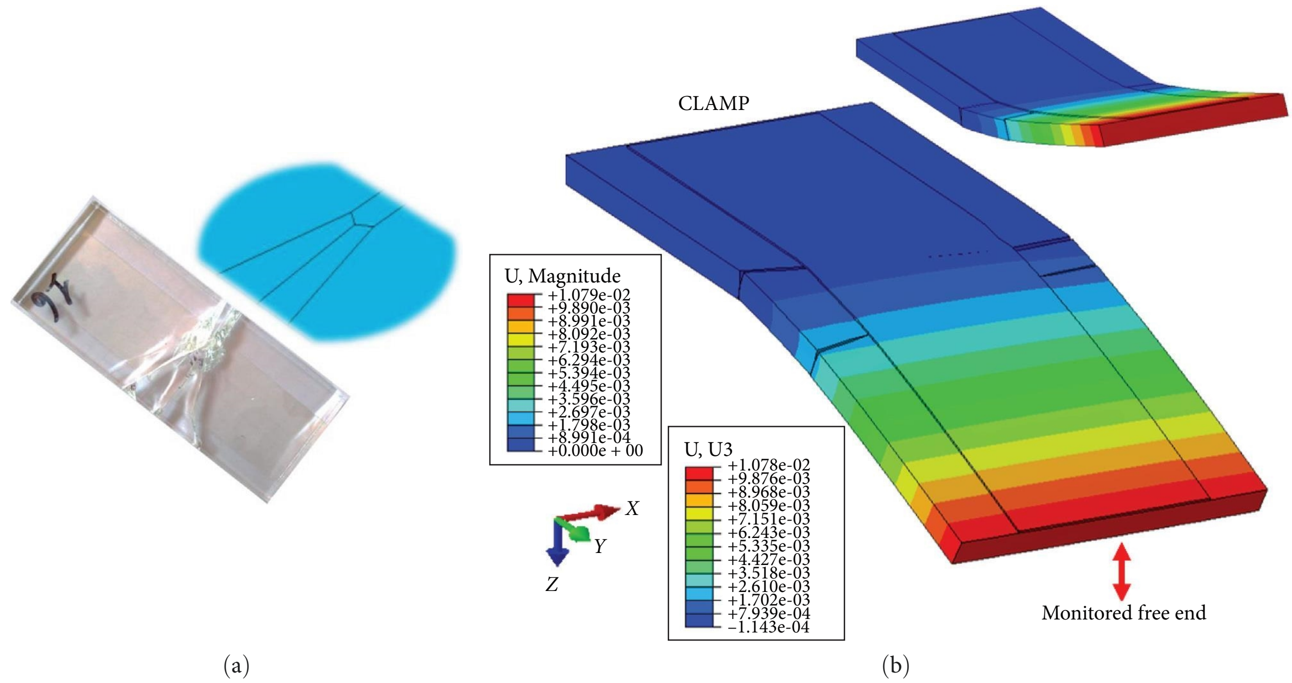

Figure 6: Full 3D solid numerical model (ABAQUS): (a) detail of crack region (photo by ©C. Bedon) and (b) typical fundamental vibration shape (with hidden mesh pattern).

Table 1: Input properties and analytical uncracked vibration frequency f_1 for the examined cantilever samples, based on Equation (1).

		Glass cantilever only	Glass + film	Glass + film + MEMS sensor
E	(GPa)	70	70*	70*
J	(mm^4)	720	720*	720*
M_{eff}	(kg)	0.01409	0.01418	0.03409
f_1	(Hz)	563.14	561.27	361.51

(*) $EJ = 87{,}074\ EJ_f$.

of K_{rot}. As a reference, for the uncracked glass specimen, Equation (1) was also used to predict the f_1 values reported in Table 1. The bending contribution of safety film (EJ_f), which was estimated up to 87,074 times smaller than glass, was rationally disregarded.

It can be seen in Table 1 that the film mass has negligible effects on f_1 (−0.33%), compared to the glass plate only, but a major sensitivity is associated to the lumped MEMS mass (−35.8%), compared to the uncracked cantilever.

As far as the K_{rot} variation is also taken into account, typical results from frequency simulations can be seen in Figure 7 (simplified ABAQUS model). The frequency trend is shown in terms of $f_{1,\mathrm{cr}}/f_1$ ratio, for the FE model earlier described in Figure 5.

When K_{rot} is numerically disregarded ($K_{\mathrm{rot}} \longrightarrow 0$, i.e., null fragments interlock), it can be rationally noted that $f_{1,\mathrm{cr}} \longrightarrow 0$ (with $f_{1,\mathrm{cr}} = 1.86$ Hz the minimum numerical frequency). Obviously, the cantilever free end is associated to bending deformations characterized by a rigid-body rotation of the bonded glass part.

Of major interest in Figure 7 is the frequency trend of the "Film" model. It can in fact be noted that the film has some mechanical effect on $f_{1,\mathrm{cr}}$ when the K_{rot} is very small (i.e., with a minimum/negligible interlock of shards), and can be mechanically disregarded for the uncracked cantilever. On the other side, the most important contribution of the film itself is to ensure any possible contact mechanisms of minor shards, and thus provide a minimum residual stiffness after fracture.

It can be noted, as a major effect of safety film, that the frequency tends to a lower bound $f_{1,\mathrm{cr}} = 19.11$ Hz, which is significantly small compared to the uncracked estimates of Table 1 (−94.11%), but still relatively high compared to the "No film" lower bound. It is also of interest to remark that the full solid FE model of Figure 6, at the lower bound, resulted in a cracked frequency $f_{1,\mathrm{cr}} = 17.86$ Hz, which is rather close to the simplified FE assembly prediction (−6.54%).

4.2. Analytical and Numerical Frequency Sensitivity to Mass Modification. For the comparative analysis of cracked frequency estimates, it is certainly important to remind that (especially for real systems) a certain mass modification can take place after repeated vibrations of fractured glass samples, as a consequence of the (possible) progressive debonding of

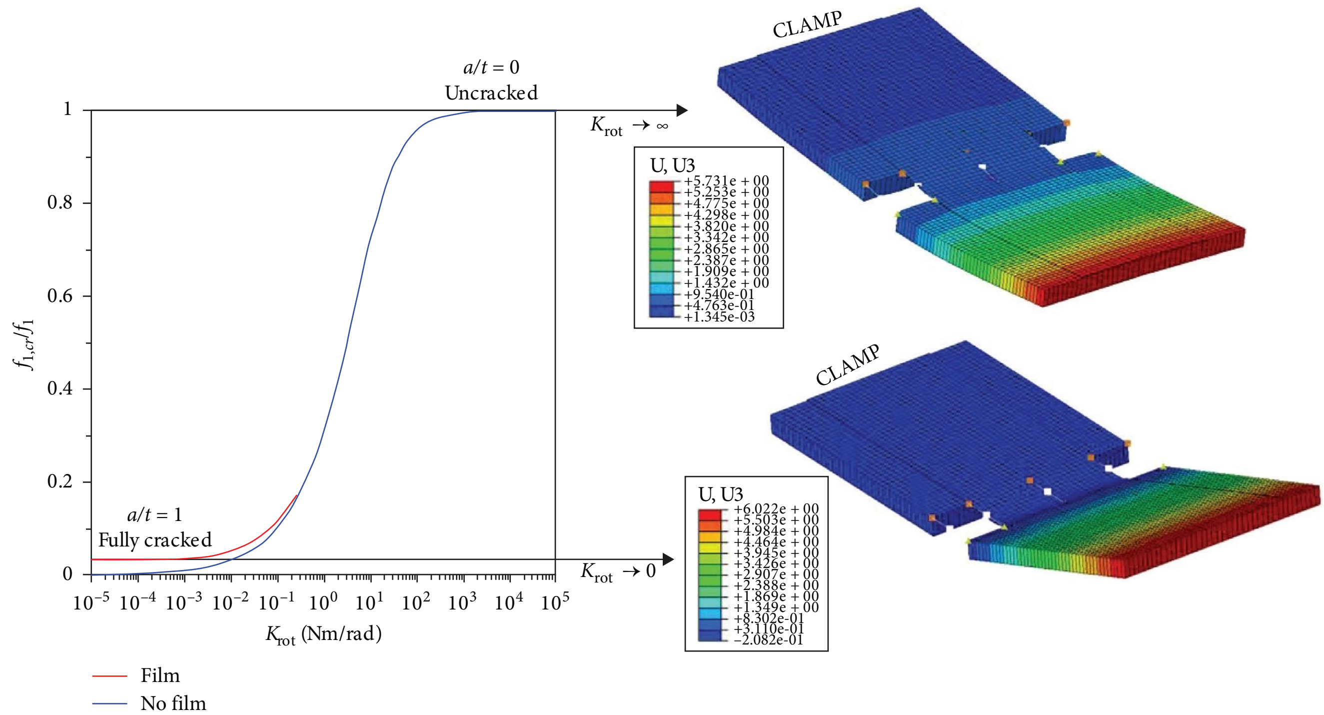

FIGURE 7: Trend of numerical cracked vibration frequency $f_{1,cr}$ for the presently examined film-bonded cantilever glass samples, as a function of K_{rot}, and expected effect of the safety film, with evidence of corresponding modal shapes (ABAQUS).

minor shards from the safety film. In most of literature studies on cracked members composed of steel or non-glass materials, see for example, in [29, 35], the mass modification ΔM from the uncracked to cracked stage is generally found very small, and can be consequently disregarded for frequency estimates. For the present experimental analysis, negligible mass reduction was encountered during the test repetitions (millimetric splinters at the interface of interlocking shards, Figure 3(c)). The mass reduction in the order of 5%–10% (Figures 3(d) and 3(e))—and thus the lack of mechanical continuity in the fractured cantilever samples—was encountered only after conclusion of the vibration tests.

In any case, it can be useful to assess the possible effect of localized mass modification in the region of major crack. To this aim, from Equation (1), the actual stiffness of the tested cantilever samples can be quantified as follows:

$$K^* = \frac{3EJ}{L_b^3}, \tag{4}$$

and M_{eff}^* in Equation (1) represents the uncracked or cracked mass.

The possible combined effect of stiffness and mass reduction on $f_{1,cr}$, based on Equation (1), can be seen in Figure 8 as a function of cracked/uncracked stiffness ratio. The $f_{1,cr}$ trend is proposed, for the total effective mass and a mass reduction of 10%, as a function of f_1 (with $\Delta M = 0$). It can be noted that $\Delta M = 10\%$ involves a constant -5.4% reduction of $f_{1,cr}$. The cracked–uncracked ratio has indeed major effects on the $f_{1,cr}$ results in Figure 8. For the lower frequency

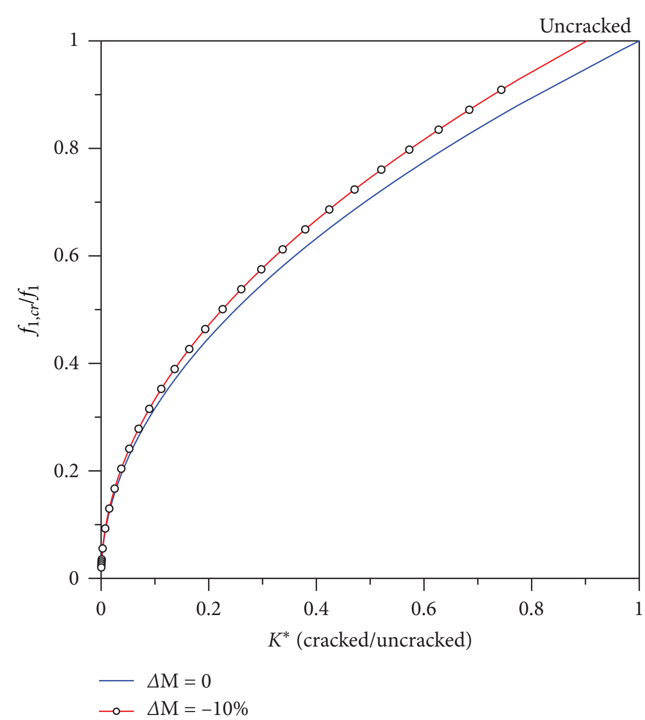

FIGURE 8: Analytical sensitivity of cracked fundamental vibration frequency, as a function of the effective stiffness K^* variation and partial mass reduction ΔM (based on Equation (1)).

bound reported in Figure 7, for example, the cracked–uncracked ratio for the equivalent bending stiffness K^* would result in about ≈0.002, for the examined samples.

TABLE 2: Summary of experimental configurations, grouped by sample/test series, with evidence of min–max acceleration range and average acceleration at the free end (in absolute value).

	Repetitions	Min acceleration $a_{\min}$ (m/s^2)	Max acceleration $a_{\max}$ (m/s^2)	Avg. acceleration a_{avg} (m/s^2)
CC#1	9	1.05	3.18	2.47 ($\pm$ 0.718)
CC#2	18	0.90	2.78	1.84 ($\pm$ 0.583)
CC#3	10	1.66	3.24	2.30 ($\pm$ 0.579)
CC#4	15	1.78	4.10	2.94 ($\pm$ 0.650)
CC#5	12	1.46	3.01	2.14 ($\pm$ 0.512)
CC#6	20	0.93	2.16	1.53 ($\pm$ 0.411)
CC#7	19	1.02	2.55	1.86 ($\pm$ 0.423)
CC#8	21	1.35	2.50	1.89 ($\pm$ 0.374)
CC#9	30	1.34	4.18	2.15 ($\pm$ 0.588)
CC#10	23	1.33	2.79	2.12 ($\pm$ 0.384)
CC#11	36	1.94	2.97	2.48 ($\pm$ 0.275)
CC#12	12	1.15	3.19	2.61 ($\pm$ 0.685)

4.3. Experimental Cracked Frequency and Acceleration. A set of records like in Figure 4 was collected and analyzed for the total 220 test repetitions (12 samples). The measured acceleration ranges are reported in Table 2 for samples grouped by test series, with evidence of maximum–minimum acceleration range, average and $\pm$ standard deviation at the free cantilever end. The corresponding $f_{1,\text{cr}}$ values are reported in Figure 9 (all samples) and in Figure 10, where they are grouped by sample, as a function of the measured acceleration peak ($a_{\max}$) for each test repetition.

Overall, based on 220 records, $f_{1,\text{cr}}$ was estimated to span between 12.22 Hz (minimum) and 21.61 Hz (maximum), with an average of 17.14 Hz ($\pm$ 2.09 Hz). The scattered distribution of experimental dots in Figure 9 is interestingly associated to a rather good linear correlation between frequency and acceleration peak estimates as follows:

$$f_{1,\text{cr}} \approx 2.35 a_{\max} + 12.08, \tag{5}$$

and $R^2 = 0.949$ the coefficient of determination (based on 220 records).

The higher is the imposed $a_{\max}$ and the higher is $f_{1,\text{cr}}$, which suggests a possible stiffening effect on the bonding film. The same effect can be noted in Figure 10, as also emphasized by the slope m of the corresponding linear fit. As a consequence of hammer-induced initial crack (with similar location and depth, but possible variations in localized minor shards), it can be seen that there is a rational scattered estimation of m, among the tested samples. Besides, the coefficient of determination of Equation (4) still suggests that there is a sound correlation among the collected results.

In terms of $f_{1,\text{cr}}$ bound and residual post-fracture stiffness for the tested specimens, it is thus of interest to focus further on the combined analysis of experimental and numerical predictions. A quantitative comparison can be found in Figure 11, where the numerical $f_{1,\text{cr}}$ outcomes (simplified model) are analyzed towards the average experimental evidences (from 220 test records). In this sense, it is worth to note that the simplified FE assembly, when $K_{\text{rot}} \longrightarrow 0$, tends to a minimum $f_{1,\text{cr}}$ which is in good correlation with the experimental average. Such a correlation confirms that the tensile behavior of glass shards (i.e., crack opening) is the most influencing parameter for post-fracture frequency considerations in similar systems, and thus the bonding film assumes a key role. This aspect was also partially observed in [18] for different setup configurations, and finds confirmation from the present experimental analysis. Further relevant considerations for future investigations, in this sense, could possibly derive from the analysis of damping and/or deformed shapes for the experimental samples.

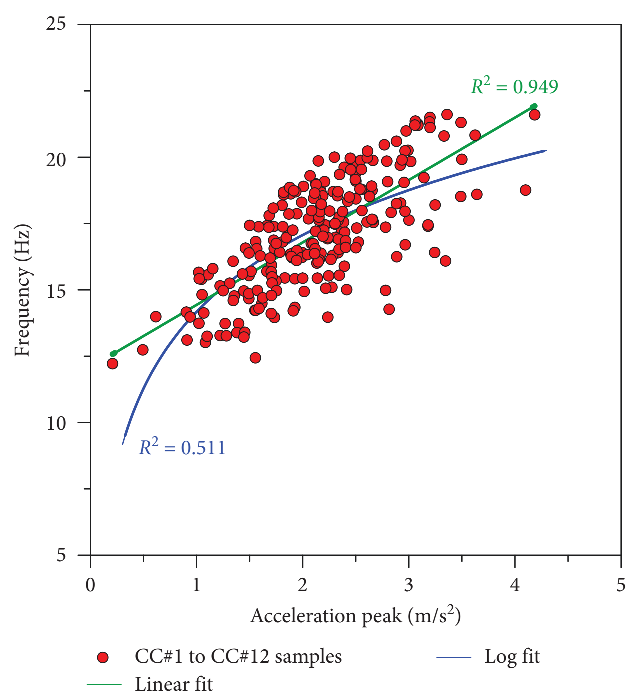

FIGURE 9: Experimental trend of cracked fundamental vibration frequency $f_{1,\text{cr}}$ for the presently examined film-bonded glass samples (all specimens and test repetitions as in Table 2), as a function of the measured acceleration peak $a_{\max}$ at the free cantilever end.

At the same time, the comparisons in Figure 11 suggest that simplified modeling strategies can be efficiently used,

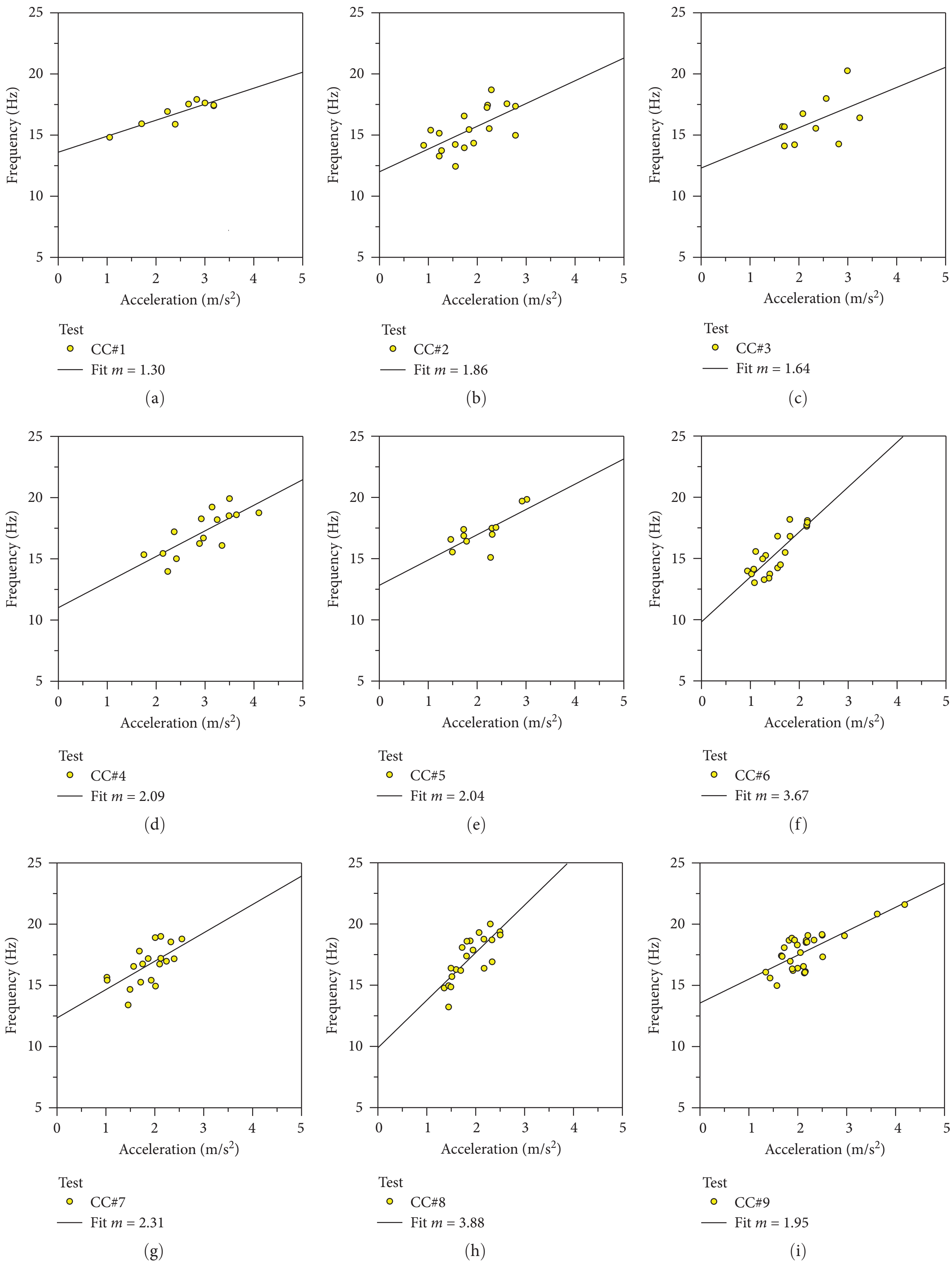

Figure 10: Continued.

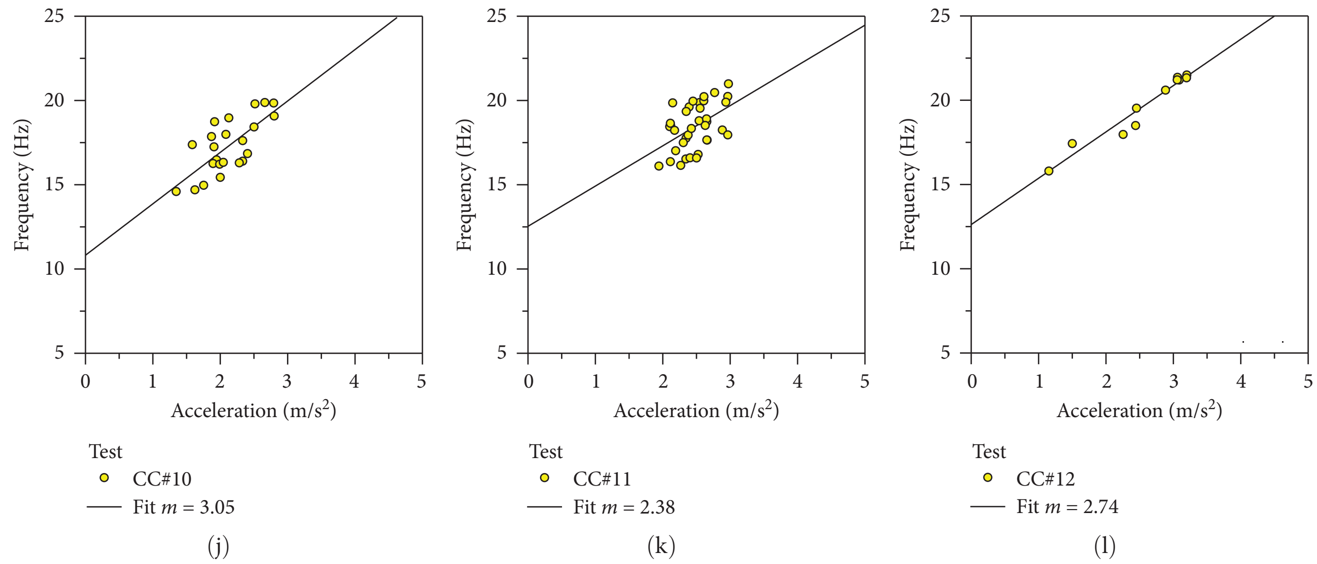

FIGURE 10: (a–m) Experimental trend of cracked fundamental vibration frequency $f_{1,cr}$ for the presently examined film-bonded cantilever glass samples, as a function of the measured acceleration peak a_{max}.

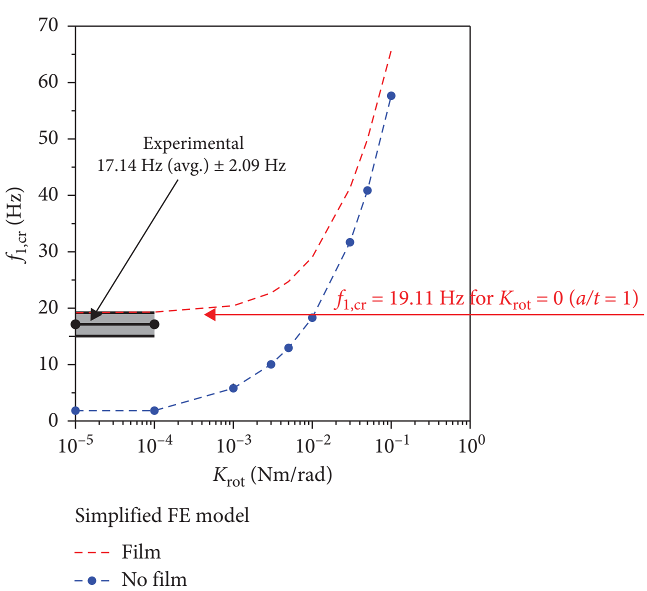

FIGURE 11: Experimental and FE numerical comparative analysis of predicted cracked vibration frequency $f_{1,cr}$ for the examined film-bonded cantilever glass samples.

upon accurate calibration, for the analysis of fractured glass components.

More precisely, the simplified FE model of Figure 5 is sufficiently realistic for the assessment of residual capacity and bending stiffness of fractured film-bonded glass samples with features and characteristics as in the present study. To note that the peak of input accelerations at the free end of specimens was measured up to $\approx 5\,m/s^2$ (Table 2 and Figure 10), at a distance of ≈50 mm from major crack, and the frequency average in Figure 11 results from 220 records. As a consequence, the present methodology could be well representative of most important dynamic features in the detailed study of fractured glass samples under repeated vibrations, to avoid (at least for preliminary estimates) more complex and uncertain FE models. At the same time, the range of experimental accelerations in Figure 11 further suggests the key role and potential of bonding films for the safety prevention in realistic critical scenarios.

4.4. Experimental Cracked Frequency and Repeated Vibrations. A final analysis of experimental evidences was carried out in terms of $f_{1,cr}$ trends as a function of test repetitions for each sample (n_v). It is reminded that a sequence of random impact magnitudes was assigned to each sample. According to Table 2, the 12 specimens were in fact subjected to an average of ≈20 test repetitions each (with a maximum of 36 for one sample only). In these conditions, Figure 12 shows the typical observations for selected specimens (CC#1, CC#10, and CC#11). It is worth to note a general decrease of $f_{1,cr}$ with n_v, for most of the samples, regardless the imposed acceleration peak a_{max}.

Also, the $f_{1,cr}$ reduction follows a rather and linear trend for all samples. Such a finding can be justified by the mostly identical mechanical properties of components, and by the strong similarity in their geometrical features.

This experimental evidence further denotes that—besides the localized interlocking phenomena of minor bonded shards—there is a rather similar post-fracture stiffness evolution and residual capacity trend for all the tested film-bonded samples. The most influencing parameter, based on Figure 12, seems associated to the progressive localized debonding of minor shards from the films in the region of crack, and thus in the progressive adjustment/rearrangement of small shards which subjected to the vibrations.

Such a localized degradation phenomenon, consequently, represents a key input parameter to quantify the load-bearing capacity after glass fracture. This is especially important for real applications, given that the present experiments were carried out in ideal laboratory conditions, and possible additional

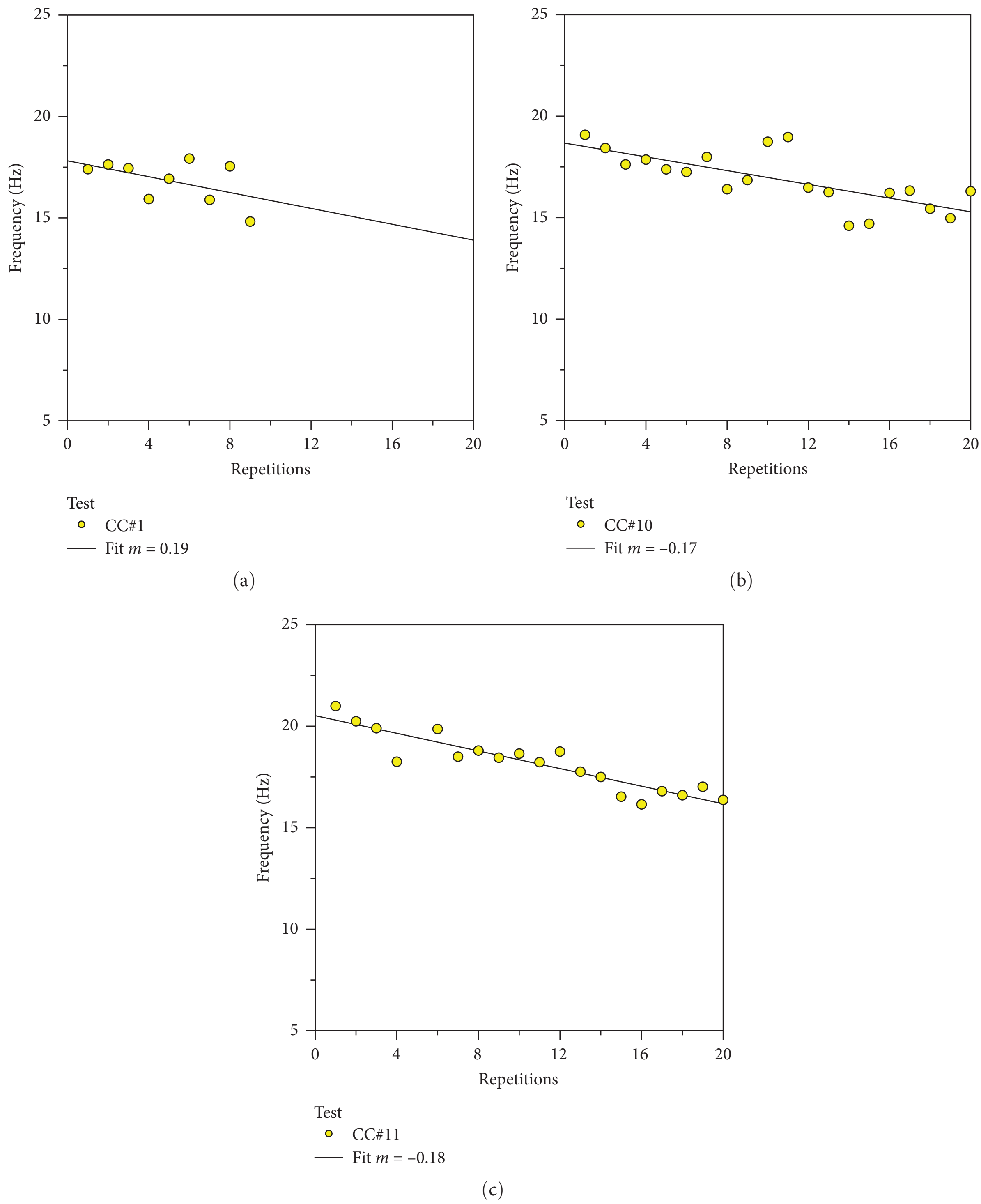

Figure 12: Experimental trend of cracked fundamental vibration frequency $f_{1,\mathrm{cr}}$ for the presently examined film-bonded cantilever glass samples, as a function of test repetitions n_ν. (a–c) denote different samples (CC#1, CC#10, and CC#11).

debond could derive from aging or unfavorable ambient conditions, or extreme mechanical loads (i.e., outside the explored range of acceleration peaks).

In terms of bonding efficiency, most importantly, some quantitative feedback could be based on the correlation of numerical/analytical and experimental frequency trends in Figure 12. As far as from Equation (1) and Figure 3, it is noted that any mass reduction (in the vibration stage) can be disregarded, the cracked frequency decrease can be rationally justified by a reduction of the effective stiffness K^*, which is found to be sensitive to $a_{\max}$, as shown in Figure 10 and Equation (4). From Figure 11, however, it can be seen that the $f_{1,\mathrm{cr}}$ reduction under random impacts is rather linearly proportional to n_ν, that is as follows:

$$f_{1,\mathrm{cr,fin}} \approx f_{1,\mathrm{cr},0} - 0.18 n_{\nu}, \tag{6}$$

with $f_{1,\mathrm{cr,fin}}$ and $f_{1,\mathrm{cr},0}$ the cracked frequency values of a single sample after n_{ν} impacts, and at the beginning of vibration tests, respectively ($n_{\nu}=1$).

Up to $n_{\nu}=20$, Equation (5) and Figure 12 reveal a typical frequency decrease down to −20%, compared to $f_{1,\mathrm{cr},0}$. Such a frequency decrease corresponds to a −35% reduction in the effective stiffness (with $\Delta M=0$), that can be also quantified as follows:

$$K^{*}_{\mathrm{fin}} \approx K^{*}{}_{0} - 4.6 n_{\nu}, \tag{7}$$

where "fin" and "0" are again defined as for Equation (5). For the presently investigated specimens, $K^{*}{}_{0}$ was approximately estimated in $0.002 \div 0.0025\ K^{*}$, compared to the uncracked stage (Figure 8).

In this sense, the current investigation further emphasizes that the post-fracture response of film-retrofitted monolithic glass samples is a rather complex and critical aspect to address. However, there are also positive outcomes to support a standard and simple assessment methodology in the existing systems. In terms of safety, such an uncertain response quantification could involve possible risk for people, given that glass fragments—in case of first fracture—are kept in position by very thin and flexible safety films. In this regard, the current experimental, analytical, and numerical study showed that—compared to the uncracked stage—the residual post-fracture stiffness (and thus load-bearing capacity) of film-retrofitted glass samples is reduced to a minimum, and under repeated vibrations can further decrease due to progressive debonding of minor glass shards. In any case, it was shown that the tested small-scale samples were able to withstand acceleration peaks up to 5 m/s^2 in the post-fracture stage, and up to ≈20 impacts with a rather stable (among the multitude of samples and repetitions) and quantifiable trend. In this sense, the experimental analysis could be further extended to full-scale samples to assess the possible extension of presently discussed observations.

5. Conclusions

In this paper, an experimental, numerical, and analytical study was presented for cracked annealed monolithic glass samples bonded by a commercial safety film of typical antishatter use for retrofit, which is based on PET-layers and PSA.

Possible safety risks for people—as a major load-bearing loss and shard fall-out—are critically dependent on the bonding efficiency of fragments. However, their residual capacity is rather challenging to quantify. To this aim, the attention and layout of laboratory experiments were focused on the analysis and track of post-fracture response and residual bending stiffness of film-bonded samples under random vibrations, based on the measurement of their cracked frequency change. In doing so, a total of 220 test repetitions were carried out on a small-scale, film-retrofitted cantilever glass plates (12 in total). Typical imposed vibrations were quantified in acceleration peaks in the range of 0.5–5 m/s^2 at the free cantilever end. The interpretation of dynamic experimental results was primarily carried out in terms of post-fracture fundamental vibration frequency (based on classical identification techniques), with the support of simplified analytical estimates, and further extended by simplified FE numerical simulations.

In terms of post-fracture performance of film-bonded glass samples in free vibrations, major effects were quantified in terms of (i) possible mass reduction (due to the accidental debonding of minor fragments), (ii) decrease of effective bending stiffness, and thus (iii) progressive decrease of the cracked vibration frequency, which is a primary performance indicator of damage severity.

For example, it was shown that:

(i) The dynamic response of tested small-scale samples was only slightly affected by a rather negligible mass modification;

(ii) On the other side, a major sensitivity was observed in the bending stiffness reduction of cracked samples, compared to the intact stage, and this effect can be efficiently captured by the frequency analysis;

(iii) Also, the progressive debond of safety film and minor glass shards (i.e., in the region of crack) was quantified (under multiple vibration tests) down to a further −35% reduction of the residual effective stiffness (for samples subjected to an average of ≈20 random impacts).

Especially under repeated vibrations, it was in fact shown that the residual mechanical performance of fractured glass elements is mostly governed by the safety film unuse, which have a key role in ensuring any mechanical contact and bending continuity between fragments. The increased number of random vibration tests, however, was generally associated to a progressive stiffness decrease, which should be properly addressed for safety considerations.

At this stage, the present analysis on small-scale samples emphasized that dynamic features are minimally sensitive to geometrical crack features. Besides, further analysis at the full-scale level is required. Detailed extended studies are needed to achieve extensive engineering knowledge on the actual capacities of retrofit solutions for structural glass applications in buildings. Finally, the present outcomes should be further extended to address the residual mechanical capacities against possible variations in the mechanical and chemical properties of bonding films (i.e., thickness, composition of layers, etc.), unfavorable ambient conditions (i.e., temperature and humidity variations, aging, etc.), or possible scale/geometrical effects (glass plates).

Data Availability

Data supporting this research article are available on request.

Conflicts of Interest

The authors declare that they have no conflicts of interest.

Acknowledgments

This research study was financially supported by the University of Trieste (“Micrograants 2020” grant). Seretti Vetroarchitetture is acknowledged for providing the monolithic glass samples.

References

[1] CEN/TC 250, “prCEN/TS xxxx-1: 2019—in-plane loaded glass components,” CEN - European Committee for Standardization, Brussels, Belgium, 2019.
[2] CEN/TC 250, “prCEN/TS xxxx-2: 2019—out of-plane loaded glass components,” CEN - European Committee for Standardization, Brussels, Belgium, 2019.
[3] C. Bedon and M. Santarsiero, “Transparency in structural glass systems via mechanical, adhesive, and laminated connections-existing research and developments,” *Advanced Engineering Materials*, vol. 20, no. 5, Article ID 1700815, 2018.
[4] K. Tserpes, A. Barroso-Caro, P. A. Carraro et al., “A review on failure theories and simulation models for adhesive joints,” *The Journal of Adhesion*, vol. 98, no. 12, pp. 1855–1915, 2022.
[5] B. Van Lancker, J. Dispersyn, W. De Corte, and J. Belis, “Durability of adhesive glass-metal connections for structural applications,” *Engineering Structures*, vol. 126, pp. 237–251, 2016.
[6] K. Machalická and M. Eliášová, “Adhesive joints in glass structures: effects of various materials in the connection, thickness of the adhesive layer, and ageing,” *International Journal of Adhesion and Adhesives*, vol. 72, pp. 10–22, 2017.
[7] C. Bedon and F. A. Santos, “Effects of post-fracture repeated impacts and short-term temperature gradients on monolithic glass elements bonded by safety films,” *Composite Structures*, vol. 319, Article ID 117166, 2023.
[8] C. Bedon, M. V. Santi, and M. Fasan, “Considerations on efficient procedural steps for seismic capacity assessment and diagnostics of historic structural glass systems,” *Soil Dynamics and Earthquake Engineering*, vol. 163, Article ID 107562, 2022.
[9] E. Volakos, C. Davis, M. Teich, P. Lenk, and M. Overend, “Structural performance of a novel liquid-laminated embedded connection for glass,” *Glass Structures & Engineering*, vol. 6, no. 4, pp. 487–510, 2021.
[10] J. Denonville, K. Puller, W. Haase, and W. Sobek, “Long-term behaviour of metal inserts partially embedded in laminated glass,” *Glasbau*, vol. 2013, pp. 117–127, 2013.
[11] C. Bedon and M. Santarsiero, “Laminated glass beams with thick embedded connections–numerical analysis of full-scale specimens during cracking regime,” *Composite Structures*, vol. 195, pp. 308–324, 2018.
[12] I. Katsivalis, O. T. Thomsen, S. Feih, and M. Achintha, “Effect of elevated temperatures and humidity on glass/steel adhesive joints,” *International Journal of Adhesion and Adhesives*, vol. 102, Article ID 102691, 2020.
[13] EN 572–2: 2004, “Glass in buildings—basic soda lime silicate glass products,” CEN, Brussels, Belgium, 2004.
[14] C. Bedon, R. Kalamar, and M. Eliášová, “Low velocity impact performance investigation on square hollow glass columns via full-scale experiments and finite element analyses,” *Composite Structures*, vol. 182, pp. 311–325, 2017.
[15] L. Figuli, C. Bedon, and D. Papan, “Experimental mechanical analysis of traditional in-service glass windows subjected to dynamic tests and hard body impact,” *Smart Structures and Systems*, vol. 27, no. 2, pp. 365–378, 2021.
[16] F. Stazi, M. Giampaoli, F. Tittarelli, C. Di Perna, and P. Munafò, “Durability of different glass coatings in humid and saline environments, ageing impact on heat-light transmission and thermal comfort,” *Building and Environment*, vol. 105, pp. 210–224, 2016.
[17] G. Mariggiò, S. Dalle Vacche, R. Bongiovanni, C. Louter, and M. Corrado, “A durable coating to prevent stress corrosion effects on the surface strength of annealed glass,” *Glass Structures & Engineering*, vol. 6, no. 4, pp. 449–462, 2021.
[18] C. Bedon and S. Mattei, “Multistep experimental calibration of mechanical parameters for modelling multilayer antishatter safety films in structural glass protection,” *Mathematical Problems in Engineering, Article ID*, vol. 2021, Article ID 6714418, 14 pages, 2021.
[19] S. Mattei, L. Cozzarini, and C. Bedon, “Experimental and numerical peeling investigation on aged multi-layer anti-shatter safety films (ASFs) for structural glass retrofit,” *Symmetry*, vol. 14, no. 1, Article ID 162, 2022.
[20] S. Mattei, L. Cozzarini, and C. Bedon, “Pre- and post-failure experimental bending analysis of glass elements coated by aged anti-shatter safety films,” *Challenging Glass Conference Proceedings*, vol. 8, pp. 1–17, 2022.
[21] A. Vedrtnam, “Experimental and simulation studies on delamination strength of laminated glass composites having polyvinyl butyral and ethyl vinyl acetate inter-layers of different critical thicknesses,” *Defence Technology*, vol. 14, no. 4, pp. 313–317, 2018.
[22] C. Bedon, “Issues on the vibration analysis of in-service laminated glass structures: analytical, experimental and numerical investigations on delaminated beams,” *Applied Sciences*, vol. 9, no. 18, Article ID 3928, 2019.
[23] A. J. Jefferson, V. Arumugam, K. Saravanakumar, H. N. Dhakal, and C. Santulli, “Compression after impact strength of repaired GFRP composite laminates under repeated impact loading,” *Composite Structures*, vol. 133, pp. 911–920, 2015.
[24] O. Ozdemir, N. Oztoprak, and H. Kandas, “Single and repeated impact behaviors of bio-sandwich structures consisting of thermoplastic face sheets and different balsa core thicknesses,” *Composites Part B: Engineering*, vol. 149, pp. 49–57, 2018.
[25] G. A. Yavuz, B. Gören Kıral, B. Hızarcı, and Z. Kıral, “Low-velocity single and repeated impact behavior of 3D printed honeycomb cellular panels,” *Materials Testing*, vol. 64, no. 10, pp. 1420–1436, 2022.
[26] P. F. Rizos, N. Aspragathos, and A. D. Dimarogonas, “Identification of crack location and magnitude in a cantilever beam from the vibration modes,” *Journal of Sound and Vibration*, vol. 138, no. 3, pp. 381–388, 1990.
[27] J. Fernández-Sáez, L. Rubio, and C. Navarro, “Approximate calculation of the fundamental frequency for bending vibrations of cracked beams,” *Journal of Sound and Vibration*, vol. 225, no. 2, pp. 345–352, 1999.
[28] J. K. Sinha, M. I. Friswell, and S. Edwards, “Simplified models for the location of cracks in beam structures using measured vibration data,” *Journal of Sound and Vibration*, vol. 251, no. 1, pp. 13–38, 2002.
[29] V. Khalkar and S. Ramachandran, “The effect of crack geometry on stiffness of spring steel cantilever beam,” *Jounral of Low Frequency Noise, Vibration and Active Control*, vol. 37, no. 4, pp. 429–455, 2018.
[30] K. H. Barad, D. S. Sharma, and V. Vyas, “Crack detection in cantilever beam by frequency based method,” *Procedia Engineering*, vol. 51, pp. 770–775, 2013.

[31] A. Vardhan and A. Singh, "Non-destructive testing based method for crack detection in beams," *Engineering Solid Mechanics*, vol. 2, no. 3, pp. 193–200, 2014.

[32] T. Lim and H. W. Park, "Investigating the modal behaviors of a beam with a transverse crack on a high-frequency bending node," *International Journal of Mechanical Sciences*, vol. 221, Article ID 107217, 2022.

[33] E. S. M. M. Soliman, "Damage severity for cracked simply supported beams," *Frattura ed Integrità Strutturale*, vol. 15, pp. 151–165, 2021.

[34] M. Chettah and R. Lassoued, "Comparative study of direct and inverse problems of cracked beams," *MATEC Web of Conferences*, vol. 149, Article ID 02015, 2018.

[35] V. Khalkar and S. Ramachandran, "Paradigm for natural frequency of an un-cracked cantilever beam and its application to cracked beam," *Journal of Engineering and Applied Sciences*, vol. 12, pp. 1714–1729, 2017.

[36] Z. Zhang, K. Shankar, E. V. Morozov, and M. Tahtali, "Vibration-based delamination detection in composite beams through frequency changes," *Journal of Vibration and Control*, vol. 22, no. 2, pp. 496–512, 2016.

[37] M. Krawczuk, W. Ostachowicz, and A. Zuk, "Analysis of natural frequencies of delaminated composite beams based on finite element method," *Structural Engineering and Mechanics*, vol. 4, no. 3, pp. 243–255, 1996.

[38] C. Bedon, M. Fasan, and C. Amadio, "Vibration analysis and dynamic characterization of structural glass elements with different restraints based on operational modal analysis," *Buildings*, vol. 9, no. 1, Article ID 13, 2019.

[39] W. M. Ostachowicz and M. Krawczuk, "On modelling of structural stiffness loss due to damage," *Key Engineering Materials*, vol. 204-205, pp. 185–200, 2001.

[40] Simulia, "Abaqus computer software," v. 6.14, 2022.

[41] S. S. Rao, *Mechanical Vibrations*, Pearson Global Edition, 2016.

[42] R. W. Clough and J. Penzien, *Dynamics of Structures*, McGraw-Hill, New York, NY, USA, 1993.

[43] MATLAB, "Version 9.4 natick; The mathWorks Inc." Natick, MA, USA, Natick, MA, USA, 2018.

[44] M. Chang, R. L. Leonard, and S. N. Pakzad, "SMIT user's guide," 2012, Release 1.0. Available online: http://smit.atlss.lehigh.edu/wp-content/uploads/2012/07/SMIT-Users-Guide.pdf.

[45] M. Chang and S. N. Pakzad, "Observer kalman filter identification for output-only systems using interactive structural modal identification toolsuite," *Journal of Bridge Engineering*, vol. 19, no. 5, Article ID 04014002, 2014.